

Surface potential-based analytical model for InGaZnO thin-film transistors with independent dual-gates*

Yi-Ni He(何伊妮), Lian-Wen Deng(邓联文)[†], Ting Qin(覃婷),
Cong-Wei Liao(廖聪维), Heng Luo(罗衡), and Sheng-Xiang Huang(黄生祥)

School of Physics and Electronics, Central South University, Changsha 410083, China

(Received 18 December 2019; revised manuscript received 29 January 2020; accepted manuscript online 13 February 2020)

An analytical drain current model on the basis of the surface potential is proposed for indium–gallium zinc oxide (InGaZnO) thin-film transistors (TFTs) with an independent dual-gate (IDG) structure. For a unified expression of carriers' distribution for the sub-threshold region and the conduction region, the concept of equivalent flat-band voltage and the Lambert W function are introduced to solve the Poisson equation, and to derive the potential distribution of the active layer. In addition, the regional integration approach is used to develop a compact analytical current–voltage model. Although only two fitting parameters are required, a good agreement is obtained between the calculated results by the proposed model and the simulation results by TCAD. The proposed current–voltage model is then implemented by using Verilog-A for SPICE simulations of a dual-gate InGaZnO TFT integrated inverter circuit.

Keywords: analytical model, independent dual-gate, indium–gallium zinc oxide (InGaZnO), surface potential

PACS: 71.23.An, 73.43.Cd, 73.20.At

DOI: 10.1088/1674-1056/ab75d2

1. Introduction

Amorphous indium–gallium zinc oxide thin film transistors (a-InGaZnO TFTs) are advantageous for the next-generation display, due to the merits of high driving ability, good reliability, and mature process over large fabrication areas.^[1–5] To further extend the applications of InGaZnO TFTs, the independent dual-gate structure is preferably adopted to adjust the threshold voltage in a wider range. Dual-gate InGaZnO TFTs render circuit response fast and power consumption low.^[6–8] Previous researches show that the threshold voltage of the driving transistor can be adjusted dynamically by discharging the auxiliary gate, which benefits good compensation effect for active matrix organic light emitting diode (AMOLED) displays.^[9] In the case of system-on-panel circuit integrations, it was proposed that high voltage–gain amplifiers be replaced by the dual-gate InGaZnO TFTs with differential inputs.^[10] Although some dual-gate InGaZnO TFT circuits were implemented and measured, there have been no mature analytical current–voltage models for dual-gate InGaZnO TFTs up to date, which brings the difficulties in designing TFTs circuit by using SPICE tools.

SPICE simulations require an analytical TFT model, which is efficient and timing saving, compared with numerical calculations.^[11,12] In recent years, the lack of appropriate analytical current–voltage model for InGaZnO TFTs attracts widespread attention from academic and industry. Perumal *et al.*^[13] presented a compact model of InGaZnO TFTs on the basis of metal–oxide–semiconductor field-effect tran-

sistor (MOSFET) SPICE model. But the model is not accurate enough. Tsuji *et al.*^[14] developed an efficient model for numerical simulations of single-gate InGaZnO TFTs. Cai *et al.*^[15] successfully developed a drain current–voltage model for dual-gate InGaZnO TFTs, which is suitable for sub-threshold and above-threshold operating regions. However, the presented model is strongly dependent on the predetermined threshold voltage, which is also difficult to calculate from physical parameters.

In this paper, an analytical current model is developed for independent dual-gate (IDG) InGaZnO TFTs on the basis of the surface potential. The effective carrier density is introduced and the Lambert function is used to solve the Poisson equation. It was proposed that the equivalent flat band voltage, *i.e.*, V_{FB} , can be used to characterize the phenomenon that the sub-threshold potential of the device is linearly modulated by the top gate voltage, *i.e.*, V_{GT} . In addition, the Lambert function is simplified by solving the potential of the sub-threshold region and the conduction region, separately. On the basis of the derived surface potential, the current–voltage expression can be derived by solving the dual integration of Pao–Sah's law. The proposed current–voltage model is applied to the SPICE simulation and validated effectively.

2. Surface potential model for IDG InGaZnO TFTs

Figure 1 shows the cross sectional view of InGaZnO TFT with independent dual-gates. The direction parallel and per-

*Project supported by the National Key Research and Development Program of China (Grant No. 2017YFA0204600) and the Fundamental Research Funds for the Central Universities of Central South University, China (Grant No. 2019zzts424).

[†]Corresponding author. E-mail: denglw@csu.edu.cn

pendicular to the TFT channel are defined as the y direction and x direction, respectively. Here t_{IGZO} , t_{OXF} , and t_{OXB} are the thickness of the InGaZnO layer, the top, and bottom gate dielectric layer, respectively. For the IDG InGaZnO TFT, the top gate voltage (V_{GT}) and bottom gate voltage (V_{GB}) are biased independently. For the simplicity of calculations, in this investigation, geometrical parameters for the top gate and bottom gate are the same, *i.e.*, thicknesses of the metal and gate insulating layer are identical.

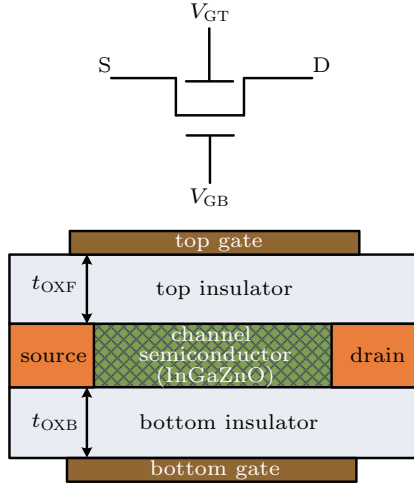


Fig. 1. The cross sectional view of independent biased dual-gate InGaZnO TFTs.

As an amorphous N-type semiconductor material, intrinsically, InGaZnO has a surface potential dependent on free electrons and localized electrons. Hence the potential of InGaZnO film follows the Poisson's equation

$$\frac{\partial^2 \varphi(x)}{\partial x^2} = -\frac{\rho(x)}{\epsilon_{\text{IGZO}}} = \frac{q}{\epsilon_{\text{IGZO}}} n_{\text{eff}}(x), \quad (1)$$

where φ is the potential along the x direction, q is the electrical charge of a single electron, ρ is the volume charge density, and ϵ_{IGZO} is the permittivity of the InGaZnO film.

Using the Boltzmann distribution function, the effective carrier density can be expressed as^[16]

$$n_{\text{eff}} = N_{\text{EFF}} \exp \left[\frac{q(\varphi - V_{\text{CH}} - \varphi_{\text{F0}})}{kT_{\text{EFF}}} \right], \quad (2)$$

where N_{EFF} is the effective carrier density, kT_{EFF} is the characteristic energy, and φ , V_{CH} , and φ_{F0} are the electrostatic potential, the channel voltage in the y direction, and the equivalent Fermi potential, respectively.

Due to the fact that

$$\partial \left[\frac{(\partial f(x)/\partial x)^2}{\partial x} \right] = 2 \frac{\partial f(x)}{\partial x} \cdot \frac{\partial^2 f(x)}{\partial x^2},$$

through solving Eq. (1), the electric field at the surface of the InGaZnO layer, *i.e.*, E_{IGZO} , can be expressed as

$$E_{\text{IGZO}} = -\sqrt{\frac{2kT_{\text{EFF}}N_{\text{EFF}}}{\epsilon_{\text{IGZO}}} \exp \left[\frac{q(\varphi_{\text{S}} - V_{\text{CH}} - \varphi_{\text{F0}})}{2kT_{\text{EFF}}} \right]}, \quad (3)$$

where φ_{S} is the surface potential.

For the interface between the gate-insulator and the InGaZnO layer, the Gaussian law can be used to relate the top and bottom gate voltage and the boundary electrical field together. Consequently, it can be derived that

$$V_{\text{GT}} = V_{\text{FB}} + \varphi_{\text{T}} - \frac{\epsilon_{\text{IGZO}}}{C_{\text{ox}}} \frac{d\varphi}{dx} \Big|_{x=0}, \quad (4a)$$

$$V_{\text{GB}} = V_{\text{FB}} + \varphi_{\text{S}} + \frac{\epsilon_{\text{IGZO}}}{C_{\text{ox}}} \frac{d\varphi}{dx} \Big|_{x=t_{\text{IGZO}}}, \quad (4b)$$

where V_{FB} is the flat-band voltage, C_{ox} is the oxide capacitance per unit area, and φ_{T} is the surface potential near the top gate. Combining Eqs. (3) and (4b), by the integration method, one can obtain that

$$\begin{aligned} & V_{\text{GB}} - V_{\text{FB}} - \varphi_{\text{S}} \\ &= \frac{\epsilon_{\text{IGZO}}}{C_{\text{ox}}} \sqrt{\frac{2kT_{\text{EFF}}N_{\text{EFF}}}{\epsilon_{\text{IGZO}}} \exp \left[\frac{q(\varphi_{\text{S}} - V_{\text{CH}} - \varphi_{\text{F0}})}{2kT_{\text{EFF}}} \right]}. \end{aligned} \quad (5)$$

However, equation (5) shows an implicit function of φ_{S} , which is not straightforward for calculations. Here the Lambert- W function is used, where $\omega = W(x)$ is the solution of the transcendental equation $\omega \cdot \exp(x) = x$. Thus, the solution of Eq. (5) can be obtained as

$$\begin{aligned} \varphi_{\text{S}} &= V_{\text{GB}} - V_{\text{FB}} - \frac{2kT_{\text{EFF}}}{q} W \left\{ \frac{q\sqrt{2kT_{\text{EFF}}N_{\text{EFF}}\epsilon_{\text{IGZO}}}}{2kT_{\text{EFF}}C_{\text{ox}}} \right. \\ &\quad \left. \times \exp \left[\frac{q(V_{\text{GB}} - V_{\text{FB}} - V_{\text{CH}} - \varphi_{\text{F0}})}{2kT_{\text{EFF}}} \right] \right\}. \end{aligned} \quad (6)$$

But the Lambert- W function cannot be embedded into SPICE simulations.^[17] According to the actually operating conditions of the IDG InGaZnO TFTs, it is possible to simplify Eq. (6). For the conduction region ($V_{\text{GB}} - V_{\text{FB}} - \varphi_{\text{F0}} > V_{\text{CH}}$), the exponential term in the W function increases rapidly. Then using the approximation that $W(x) = \ln(x) - \ln(\ln(x))$,^[18] φ_{S} can be expressed as

$$\begin{aligned} \varphi_{\text{S}} &= V_{\text{CH}} + \varphi_{\text{F0}} + \frac{2kT_{\text{EFF}}}{q} \ln \left\{ \frac{2kT_{\text{EFF}}C_{\text{ox}}}{q\sqrt{2kT_{\text{EFF}}N_{\text{EFF}}\epsilon_{\text{IGZO}}}} \right. \\ &\quad \times \left[\ln \left(\frac{q\sqrt{2N_{\text{EFF}}\epsilon_{\text{IGZO}}kT_{\text{EFF}}}}{2kT_{\text{EFF}}C_{\text{ox}}} \right) \right. \\ &\quad \left. \left. + \frac{q(V_{\text{GB}} - V_{\text{FB}} - V_{\text{CH}} - \varphi_{\text{F0}})}{2kT} \right) \right] \right\}. \end{aligned} \quad (7)$$

On the other hand, for the sub-threshold region ($V_{\text{GB}} - V_{\text{FB}} - \varphi_{\text{F0}} < V_{\text{CH}}$), the exponential term in the W function approaches to 0. In addition, due to the observed linear relationship between φ_{S} and the top gate bias voltage V_{GT} , φ_{S} can be expressed as

$$\varphi_{\text{S}} = \lambda(V_{\text{GB}} - V_{\text{FB}}), \quad (8)$$

where λ depends on the ratio of the equivalent capacitance of the gate oxide layer to that of the active layer, which represents

the modulation extent of V_{GB} for φ_S ; V_{FB} is the equivalent flat band voltage, which can be divided into V_{FB1} and V_{FB2} . Here V_{FB1} represents the difference in work function between the gate metal and InGaZnO layer, and V_{FB2} denotes the influence of the oxide layer and interface charge. As the carrier concentration of InGaZnO layer is modulated by V_{GT} , the V_{FB} can be expressed as

$$V_{FB} = V_{FB1} + V_{FB2} = V_{FB1} + a \cdot V_{GT}. \quad (9)$$

For a continuous expression of surface potential for IDG InGaZnO TFT with different operating regimes, equations (8) and (9) can be combined through a smoothing function of $\tanh x$, then φ_S is expressed as

$$\begin{aligned} \varphi_S = & 0.5 \{1 - \tanh[10(V_{GB} - V_{FB} - V_{CH} - \varphi_{F0})]\} \\ & \times [\lambda \cdot (V_{GB} - V_{FB1} - a \cdot V_{GT})] \\ & + 0.5 \{1 + \tanh[10(V_{GB} - V_{FB} - V_{CH} - \varphi_{F0})]\} \\ & \times \left\{ V_{CH} + \varphi_{F0} + \frac{2kT_{EFF}}{q} \cdot \ln \frac{2kT_{EFF}C_{ox}}{q\sqrt{2kT_{EFF}N_{EFF}\epsilon_{IGZO}}} \right. \\ & \times \left[\ln \frac{q\sqrt{2kT_{EFF}N_{EFF}\epsilon_{IGZO}}}{2kT_{EFF}C_{ox}} \right. \\ & \left. \left. + \frac{q(V_{GB} - V_{FB} - V_{CH} - \varphi_{F0})}{2kT_{EFF}} \right] \right\}. \quad (10) \end{aligned}$$

3. Drain current model of IDG InGaZnO TFT

On the basis of the obtained analytical surface potential, the current-voltage model for IDG InGaZnO TFT is developed as follows. According to the Pao-Sah formula, the drain-source current of the IDG InGaZnO TFT is

$$I_{DS} = \frac{W}{L} \int_0^{V_{DS}} \int_{\varphi_T}^{\varphi_S} \mu_{EFF} \frac{q \cdot n_{EFF}}{E} d\varphi \cdot dV_{CH}, \quad (11)$$

where μ_{EFF} is the effective mobility, W and L represent the width and length of the TFT. According to the previous investigations, the stretch-exponential function is consistent well with the curves of measured effective mobility *versus* gate-source voltage, thus

$$\mu_{EFF} = \mu_{BAND} \cdot \{1 - \exp[-(V_{GB} - V_{FB})^m]\}, \quad (12)$$

where m is the shape fitting parameter for the curve of mobility *versus* V_{GB} .

Then the partial derivative of E (Eq. (3)) with respect to the channel voltage (*i.e.*, V_{CH}) is given as

$$\frac{\partial E}{\partial V_{CH}} = -\frac{1}{E} \frac{qN_{EFF}}{\epsilon_{IGZO}} \exp[\beta(\varphi - V_{CH} - \varphi_{F0})]. \quad (13)$$

Substituting Eqs. (12) and (13) into Eq. (11), one can obtain

$$\begin{aligned} I_{DS} = & \frac{W}{L} \mu_{BAND} \cdot \epsilon_{IGZO} \cdot \{1 - \exp[-(V_{GB} - V_{FB})^m]\} \\ & \times \int_0^{V_{DS}} \int_{\varphi(x=\epsilon_{IGZO})}^{\varphi_S} \left(-\frac{\partial E}{\partial V_{CH}} \right) d\varphi \cdot dV_{CH}. \quad (14) \end{aligned}$$

Figure 2 demonstrates the comparison of the TCAD simulated and calculated φ_S and φ_T *versus* channel voltage, from $V_{CH} = 0$ to $V_{CH} = V_{DS}$. It is observed that the calculated and the simulations results are in good agreement with each other. According to Eq. (14), figure 2 shows the integration boundaries. By dividing the integration regions, I_{DS} can be derived as

$$\begin{aligned} I_{DS} = & -\frac{W}{L} \mu_{BAND} \cdot \epsilon_{IGZO} \cdot \{1 - \exp[-(V_{GB} - V_{FB})^m]\} \\ & \times \int_0^{V_{DS}} \int_{\varphi_T}^{\varphi_S} \frac{\partial E}{\partial V_{CH}} d\varphi \cdot dV_{CH} \\ = & -\frac{W}{L} \mu_{BAND} \cdot \epsilon_{IGZO} \{1 - \exp[-(V_{GB} - V_{FB})^m]\} \\ & \times \left\{ \int_0^{V_{DS}} \int_{\varphi_{T0}}^{\varphi_{S0}} \frac{\partial E}{\partial V_{CH}} d\varphi \cdot dV_{CH} \right. \\ & + \int_0^{V_{DS}} \int_{\varphi_{S0}}^{\varphi_S} \frac{\partial E}{\partial V_{CH}} d\varphi \cdot dV_{CH} \\ & \left. - \int_0^{V_{DS}} \int_{\varphi_{T0}}^{\varphi_T} \frac{\partial E}{\partial V_{CH}} d\varphi \cdot dV_{CH} \right\} \\ = & -\frac{W}{L} \mu_{BAND} \cdot \epsilon_{IGZO} \cdot \{1 - \exp[-(V_{GB} - V_{FB})^m]\} \\ & \times \left\{ \int_{\varphi_{TL}}^{\varphi_{SL}} E(\varphi, V_{CH} = V_{DS}) d\varphi - \int_{\varphi_{T0}}^{\varphi_{S0}} E(\varphi, V_{CH} = 0) d\varphi \right. \\ & - \int_{\varphi_{S0}}^{\varphi_{SL}} E(\varphi, V_{CH} = V_S) d\varphi \\ & \left. + \int_{\varphi_{T0}}^{\varphi_{TL}} E(\varphi, V_{CH} = V_T) d\varphi \right\}. \quad (15) \end{aligned}$$

By directly integrating Eq. (3), the first and second terms on the right-hand side of Eq. (15) can be derived as

$$\begin{aligned} & \int_{\varphi_{TL}}^{\varphi_{SL}} E(\varphi, V_{CH} = V_{DS}) d\varphi \\ = & \int_{\varphi_{TL}}^{\varphi_{SL}} \sqrt{\frac{2N_{EFF}kT_{EFF}}{\epsilon_{IGZO}}} \exp \frac{q(\varphi - V_{DS} - \varphi_{F0})}{2kT_{EFF}} d\varphi \\ = & \frac{2kT_{EFF}}{q} \sqrt{\frac{2N_{EFF}kT_{EFF}}{\epsilon_{IGZO}}} \exp \frac{q(-V_{DS} - \varphi_{F0})}{2kT_{EFF}} \\ & \times \left(\exp \frac{q\varphi_{SL}}{2kT_{EFF}} - \exp \frac{q\varphi_{TL}}{2kT_{EFF}} \right), \quad (16) \end{aligned}$$

$$\begin{aligned} & \int_{\varphi_{T0}}^{\varphi_{S0}} E(\varphi, V_{CH} = 0) d\varphi \\ = & \int_{\varphi_{T0}}^{\varphi_{S0}} \sqrt{\frac{2N_{EFF}kT_{EFF}}{\epsilon_{IGZO}}} \exp \frac{q(\varphi - \varphi_{F0})}{2kT_{EFF}} d\varphi \\ = & \frac{2kT_{EFF}}{q} \sqrt{\frac{2N_{EFF}kT_{EFF}}{\epsilon_{IGZO}}} \exp \frac{q(-\varphi_{F0})}{2kT_{EFF}} \\ & \times \left(\exp \frac{q\varphi_{S0}}{2kT_{EFF}} - \exp \frac{q\varphi_{T0}}{2kT_{EFF}} \right). \quad (17) \end{aligned}$$

By combining Eq. (4a) and Eq. (4b), the third and fourth integral terms of Eq. (15) can be derived as

$$\int_{\varphi_{S0}}^{\varphi_{SL}} E(\varphi, V_{CH} = V_S) d\varphi$$

$$\begin{aligned}
 &= \int_{\varphi_{S0}}^{\varphi_{SL}} \frac{C_{ox}}{\epsilon_{IGZO}} (V_{GB} - V_{FB} - \varphi) d\varphi \\
 &= \frac{C_{ox}}{\epsilon_{IGZO}} \left[(V_{GB} - V_{FB})(\varphi_{SL} - \varphi_{S0}) - \frac{1}{2}(\varphi_{SL}^2 - \varphi_{S0}^2) \right], \quad (18)
 \end{aligned}$$

$$\begin{aligned}
 &\int_{\varphi_{T0}}^{\varphi_{TL}} E(\varphi, V_{CH} = V_T) d\varphi \\
 &= \int_{\varphi_{T0}}^{\varphi_{TL}} \frac{-C_{ox}}{\epsilon_{IGZO}} (V_{GT} - V_{FB} - \varphi) d\varphi \\
 &= -\frac{C_{ox}}{\epsilon_{IGZO}} \left[(V_{GT} - V_{FB})(\varphi_{TL} - \varphi_{T0}) - \frac{1}{2}(\varphi_{TL}^2 - \varphi_{T0}^2) \right]. \quad (19)
 \end{aligned}$$

Consequently, the analytical expression for the I_{DS} of IDG InGaZnO TFT is

$$\begin{aligned}
 I_{DS} &= \frac{W}{L} \mu_{EFF} \cdot \epsilon_{IGZO} \cdot \{1 - \exp[-(V_{GB} - V_{FB})^m]\} \\
 &\times \left\{ -\frac{2kT_{EFF}}{q} \sqrt{\frac{2N_{EFF}kT_{EFF}}{\epsilon_{IGZO}}} \exp\left(\frac{q(-V_{DS} - \varphi_{F0})}{2kT_{EFF}}\right) \right. \\
 &\times \left(\exp\left(\frac{q\varphi_{SL}}{2kT_{EFF}}\right) - \exp\left(\frac{q\varphi_{TL}}{2kT_{EFF}}\right) \right) \\
 &+ \frac{2kT_{EFF}}{q} \sqrt{\frac{2N_{EFF}kT_{EFF}}{\epsilon_{IGZO}}} \exp\left(\frac{q(-\varphi_{F0})}{2kT_{EFF}}\right) \\
 &\times \left(\exp\left(\frac{q\varphi_{S0}}{2kT_{EFF}}\right) - \exp\left(\frac{q\varphi_{T0}}{2kT_{EFF}}\right) \right) \\
 &+ \frac{C_{ox}}{\epsilon_{IGZO}} \left[(V_{GB} - V_{FB})(\varphi_{SL} - \varphi_{S0}) - \frac{1}{2}(\varphi_{SL}^2 - \varphi_{S0}^2) \right] \\
 &\left. + \frac{C_{ox}}{\epsilon_{IGZO}} \left[(V_{GT} - V_{FB})(\varphi_{TL} - \varphi_{T0}) - \frac{1}{2}(\varphi_{TL}^2 - \varphi_{T0}^2) \right] \right\}. \quad (20)
 \end{aligned}$$

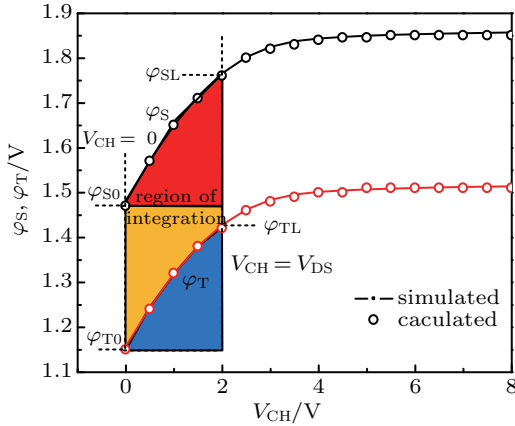


Fig. 2. Plots of surface potential φ_S and top potential φ_T versus channel voltage for IDG InGaZnO TFT, with colored area referring to integration region.

4. Results and discussion

To verify the developed model, comparisons are carried out between the calculated and TCAD simulated results. The investigated TFT structure is shown in Fig. 1, and the V_{GT} and the V_{GB} are biased independently. Listed in Table 1 are the physical and geometrical parameters to calculate the current-voltage curve for IDG InGaZnO TFTs.

Table 1. InGaZnO TFT parameters for TCAD simulation and model calculation.

Parameter/units	Value
$C_{ox}/(\text{nF}/\text{cm}^2)$	17.26
t_{IGZO}/nm	40
$W/\mu\text{m}$	60
$L/\mu\text{m}$	10
t_{ox}/nm	200
ϵ_{rIGZO}	12.31
kT/eV	0.026
N_{EFF}/cm^{-3}	5.53×10^{-18}
λ	0.5
a	-1
m	2

Figure 3 shows the comparison between the calculated surface potential using Eq. (9) and the simulated surface potential. The potential of the sub-threshold region is shifted with V_{GT} increasing, but the slope of sub-threshold surface potential remains unchanged approximately till V_{GT} reaches to 0.5 V. Under various biasing conditions, the calculated values of φ_S in good agreement with the simulated ones.

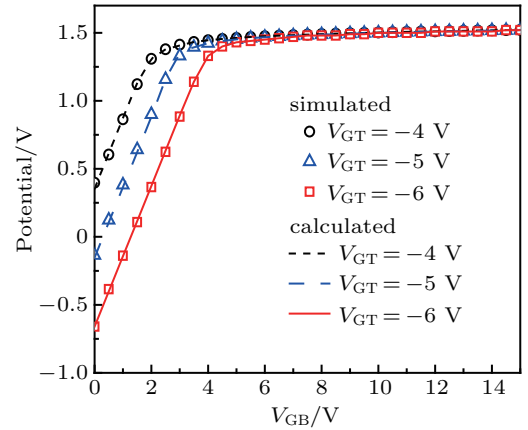


Fig. 3. Simulated and calculated plots of surface potential φ_S versus bottom gate voltage V_{GB} for three different values of V_{GT} .

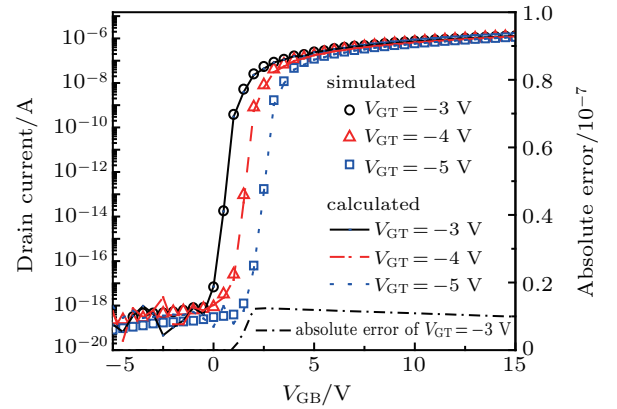


Fig. 4. Comparison between simulated and calculated transfer characteristics of IDG a-InGaZnO TFT for three different values of V_{GT} .

Figure 4 shows the comparison results of the simulated and calculated drain-source current versus V_{GB} for different

values of V_{GT} . Further, the calculated and simulated output characteristics of IDG InGaZnO TFT are shown in Fig. 5. For both the transfer and output characteristics, the proposed model shows a high consistence with TCAD simulations, and the absolute error is less than 10^{-8} . It is demonstrated that the threshold voltage of InGaZnO TFT can be adjusted using the independent biased gate electrode. With the decrease of V_{GT} , the threshold voltage shifts positively, because more charges in the InGaZnO film are depleted.

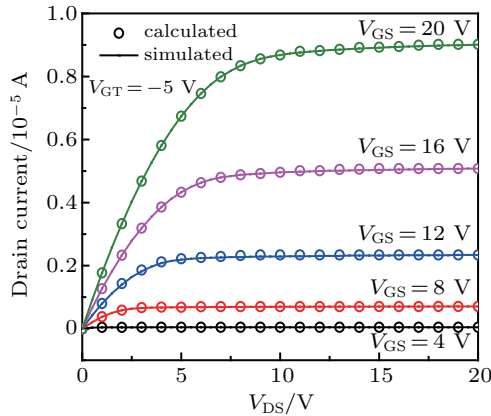


Fig. 5. Comparison between calculated and simulated output characteristics of IDG a-InGaZnO TFT with $V_{GT} = -5$ V for various values of V_{GS} .

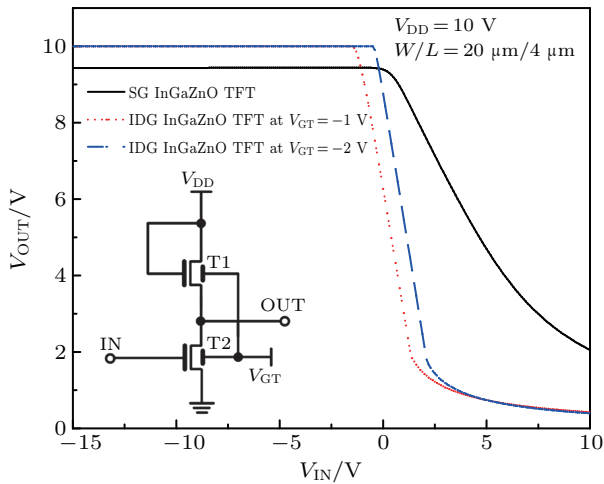


Fig. 6. Comparison results between SG and IDG InGaZnO TFTs using Verilog-A model, with inset schematically showing inverter circuit with IDG InGaZnO TFTs.

The proposed model is integrated into circuit simulations with Verilog-A. Figure 6 shows the HSPICE simulation comparison results of an InGaZnO TFT inverter with single-gate (SG) and independent dual-gate (IDG). The power supply (V_{DD}) is 10 V, and V_{GT} for the IDG transistor is -1 V and -2 V, respectively. It is observed that increased output swing

and narrower transient region can be obtained by the IDG transistors.

5. Conclusions

In this work, an analytical drain current model for independent dual-gate InGaZnO TFT is established based on the surface potential. Equivalent flat band voltage V_{FB} is introduced to represent the linear surface potential modulation effect of the top gate voltage V_{GT} . Following the Pao-Sah's law, regional integration is carried out in detail to obtain a continuous current-voltage model for the independent dual-gate InGaZnO TFTs. Comparisons between the model calculations and the TCAD simulations are carried out, and the results show that both the transfer and output characteristics are in good agreement for different operation regions. Furthermore, in order to verify the effectiveness of IDG InGaZnO TFTs for high-performance circuit designs, the model is applied to an SPICE simulator using Verilog-A, which is helpful in designing the high performance InGaZnO TFT circuit for system on panel circuit integrations.

References

- [1] Fortunato E, Barquinha P and Martins R 2012 *Adv. Mater.* **24** 2945
- [2] Feng G D, Zhao Y H and Jiang J 2019 *Solid State Electron.* **153** 16
- [3] Hu W N, Jiang J, Xie D D, Wang S T, Bi K X, Duan H G, Yang J L and He J 2018 *Nanoscale* **10** 14893
- [4] Lan L F, Dai X Q, He C C, Liu L, Yang X B, Liang L Y, Cao H T and Peng J B 2019 *IEEE Trans. Electron Dev.* **66** 2620
- [5] Song E L, Lan L F, Xiao P, Lin Z G, Sun S, Li Y Z, Song W, Gao P X and Peng J B 2016 *IEEE Trans. Electron Dev.* **63** 1916
- [6] Qin T, Huang S X, Liao C W, Yu T B, Luo H, Liu S and Deng L W 2018 *Acta Phys. Sin.* **66** 097101 (in Chinese)
- [7] Zan H W, Li C H and Yeh C C 2011 *Appl. Phys. Lett.* **98** 253503
- [8] Qin T, Liao C W, Huang S X, Yu T B and Deng L W 2018 *Jpn. J. Appl. Phys.* **57** 014301
- [9] Zaidi W, Costa J, Pouryazdan A, Abdullah W and Münzenrieder N 2018 *IEEE Electron Dev. Lett.* **39** 1314
- [10] Tai Y H, Chiu H L, Chou L S and Chang C H 2012 *IEEE Electron Dev. Lett.* **33** 1729
- [11] Park J H, Lee S, Jeon K, Kim S, Kim S, Park J, Song I, Kim C J, Park Y, Kim D M and Kim D H 2009 *IEEE Electron Dev. Lett.* **30** 1069
- [12] Jeon K, Kim C J, Song I, Park J, Kim S, Kim S, Park Y, Park J H, Lee S, Kim D M and Kim D H 2008 *Appl. Phys. Lett.* **93** 182102
- [13] Perumal C, Ishida K, Shabanpour R, Boroujeni B K, Petti L, Münzenrieder N, Salvatore G A, Carta C, Tröster G and Ellinger F 2013 *IEEE Electron Dev. Lett.* **34** 1391
- [14] Tsuji H, Nakata M, Sato H, Nakajima Y, Fujisaki Y, Takei T, Fujikake H, Yamamoto T and Shimidzu N 2014 *J. Disp. Technol.* **10** 101
- [15] Cai M X and Yao R H 2018 *Sci. Chin. (Inf. Sci.)* **61** 022401
- [16] Qin T, Huang S X, Liao C W, Yu T B and Deng L W 2017 *Acta Phys. Sin.* **57** 014301 (in Chinese)
- [17] Alvarado J, Iñiguez B, Estrada M, Flandre D and Cerdeira A 2010 *Int. J. Number. Model. Electron. Netw. Dev. Fields* **23** 88
- [18] Hoorfar A and Hassani M 2008 *J. Inequalities Pure Appl. Math.* **9** 5